THEORETICAL SIMULATION OF A ROOM TEMPERATURE HgCdTe LONG-WAVE DETECTOR FOR FAST RESPONSE – OPERATING UNDER ZERO BIAS CONDITIONS

Piotr Martyniuk, Małgorzata Kopytko, Paweł Madejczyk, Aleksandra Henig, Kacper Grodecki, Waldemar Gawron, Jarosław Rutkowski

Military University of Technology, Institute of Applied Physics, Gen. S. Kaliskiego 2, 00-908 Warsaw, Poland
(✉ piotr.martyniuk@wat.edu.pl, +48 26 183 9215, malgorzata.kopytko@wat.edu.pl, pawel.madejczyk@wat.edu.pl, aleksandra.henig@wat.edu.pl, kacper.grodecki@wat.edu.pl, wgawron@vigo.com.pl, jaroslaw.rutkowski@wat.edu.pl)

Abstract

The paper reports on a long-wave infrared (cut-off wavelength ~ 9 μm) HgCdTe detector operating under unbiased condition and room temperature (300 K) for both short response time and high detectivity operation. The optimal structure in terms of the response time and detectivity versus device architecture was shown. The response time of the long-wave (active layer Cd composition, $x_{Cd} = 0.19$) HgCdTe detector for 300 K was calculated at a level of $\tau_s \sim 1$ ns for zero bias condition, while the detectivity – at a level of $D^* \sim 10^9$ cmHz$^{1/2}$/W assuming immersion. It was presented that parameters of the active layer and P$^+$ barrier layer play a critical role in order to reach $\tau_s \leq 1$ ns. An extra series resistance related to the *processing* (R_{S+} in a range 5−10 Ω) increased the response time more than two times ($\tau_s \sim 2.3$ ns).

Keywords: response time, unbiased condition, HgCdTe, LWIR, higher operating temperature.

1. Introduction

The room operating temperature condition of long-wave (8−12 μm, LWIR) detectors is the key research area in the infrared technology covering many applications [1]. Those new applications directly contribute to stringent (especially for zero bias and room temperature $T \sim 300$ K) operating conditions – a short response time (< 1 ns) and a high detectivity corresponding to the background limited photodetector – BLIP (> 10^9 cmHz$^{1/2}$/W) [2]. The requirement of the zero bias structures is mostly related to the fact that biased structures operating under non-equilibrium conditions exhibit an increase of 1/f noise, while the lack of cooling reduces the cost of the devices [3]. According to the experimental results presented in our previous papers, the LWIR HgCdTe N$^+\pi$P$^+$n$^+$ (π stands for a low doped p-type active layer) photodetectors operating under non-equilibrium conditions and room temperature reach a response time in a several nanosecond range and an optimized detectivity (p type absorber's doping < 10^{16} cm^{-3}) – $D^* \sim 10^{10}$ cmHz$^{1/2}$/W (assuming that the detector is immersed) [4−8].

For unbiased structures a fast loss in a signal due to a high rate of recombination in the absorber region and a very short passage time of carriers through the depletion area play the decisive role in ultra-fast response operation. To fabricate a detector exhibiting both short response time and high detectivity operating under zero bias conditions, multilayer hetero-structures must be implemented. In terms of a short response time, the p-type absorber is more useful due to high carrier ambipolar mobility. Additionally, in terms of reaching a high detectivity, in the fundamental approach, the p-type HgCdTe active regions exhibit the best

compromise between the requirement of high quantum efficiency and a low thermal *generation-recombination* (GR) rate [9]. The mentioned complex multi-layer structures should consist of proper doping and composition gradient layers. Our main contribution to the field in comparison with the well-known three-layer N^+pP^+ structure invented and introduced by Elliot *et al.* for non-equilibrium conditions is intentional doping and composition gradient layers at heterojunctions (interfaces) [10−17].

The paper deals with the theoretical simulation of a photodetector for fast response conditions (< 1 ns) based on epitaxial HgCdTe multi-layer graded gap architecture. The detector structure was simulated with APSYS software by Crosslight Inc. [18]. A time response of the LWIR HgCdTe detector with the active layer composition $x_{Cd} = 0.19$ at $T = 300$ K was estimated at a level of $\tau_s \sim 1$ ns for a series resistance $R_S = 0.77\ \Omega$ (an extra series resistance $R_{S+} = 0\ \Omega$). It was shown that the extra series resistance, related to the *processing* (R_{S+} in the range 5−10 Ω) increased the response time more than two times ($\tau_s \sim 2.3$ ns) for zero bias condition.

2. Architecture for unbiased condition

A graph of the simulated multilayer $N^+pP^+n^+$ structure for unbiased condition and operating in room temperature exhibiting both short response time and high detectivity is presented in Fig. 1, where detailed input parameter values of included gradient layers (interface layers) with proper doping and composition gradients are shown. Other parameters taken in modelling of LWIR detector are presented in Table 1. As mentioned above, the highly doped *p*-type active layer will be preferable to meet the requirement of a short time response. Both N^+ and P^+ wide bandgap barrier layers should be highly doped ($N_D, N_A > 10^{17}$ cm^{-3}) to minimize the diffusion length for carriers generated in regions close to the electric contacts and device resistance. Additionally, a highly doped n^+ ($N_D > 10^{17}$ cm^{-3}) layer provides a low resistance contact to metallization. In addition, the N^+ contact/barrier layer plays also the role of a radiation window and should be chosen in relation to absorber in terms of x_{Cd} to determine an appropriate cut-on wavelength of the photodetector.
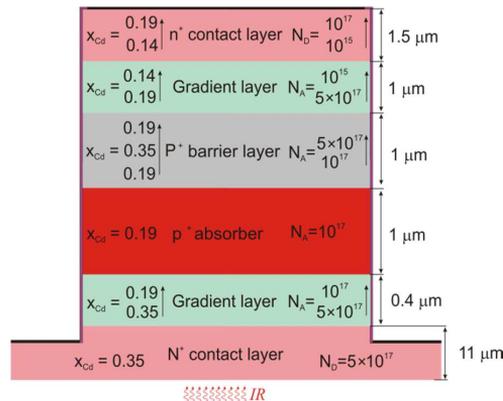

Fig. 1. The simulated HgCdTe multilayer $N^+pP^+n^+$ structure. Layers' N_D, N_A doping in cm^{-3}.

Optimization regarding a short response time and high detectivity is difficult due to the fact that both parameters rule out one another. Since the detector operates under zero bias, it was assumed that detectivity was limited by thermal Johnson-Nyquist noise. In addition, the structure could be optimized in terms of a short response time without a significant reduction in detectivity by assuming the immersion effect increasing detectivity by $\sim n^2$, where *n* stands for the GaAs substrate refractive index, according to the relation:

$$D^* = \frac{n^2 R_i}{(4k_B T/R_o A)^{0.5}},$$

(1)

where: R_i, k_B, R_o, A stand for current responsivity, the Boltzmann constant, a resistance at zero bias and the detector's electrical area, respectively. In terms of a response time the photocurrent dependence on time was used, where time for a $1/e$ drop from the photocurrent's maximum value was assessed.

The dependence of the response time and detectivity on the complex multilayer architecture, *i.e.* x_{Cd} composition, d thickness, N_A, N_D doping of a single layer and doping gradients, was simulated. In addition, the dependencies of the structure resistance and capacitance on the structural parameters were presented. The numerical simulation of the HgCdTe multilayer hetero-structure was performed by APSYS platform (Crosslight Inc.). The numerical model implemented in APSYS platform incorporates HgCdTe GR mechanisms. The absorption's coefficient (α), temperature, doping and composition dependence were assumed (for $T = 300$ K and active layer composition, $x_{Cd} = 0.19$, $\alpha = 137923$ m^{-1}). All equations describing GR models and parameters as intrinsic concentration, bandgap energy, carrier mobility, dielectric constants used in simulations were taken after the monograph by Capper and the APSYS manual [18−20]. The model given by Li *et al.* used in response time calculation and simulation was performed for $\lambda = 8$ μm [21].

Table 1. The parameters taken in modelling of LWIR detector.

Parameter	Symbol	Value
N_D, N_A – doping gauss tail	dx [μm]	0.02
trap density	N_T [cm^{-3}]	10^{14}
trap energy level	E_T	1/3 E_g (with respect to E_c)
capture coefficients SRH recombination centers	c_n, c_P [cm^3 s^{-1}]	1.5×10^{-7}, 3×10^{-9}
detector's electrical area	A [μm^2]	100×100
overlap integrals for Bloch functions	$F_1 F_2$	0.3
incident power density	P [W m^{-2}]	500

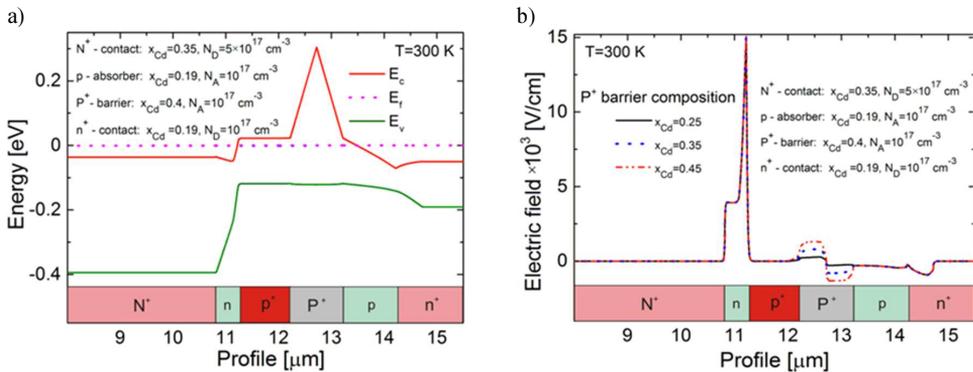a)   b)

Fig. 2. The energy band profile (a) and the electric field (b) at HgCdTe multilayer N$^+$pP$^+$n$^+$ structure calculated for $T = 300$ K; N$^+$ contact $x_{Cd} = 0.35$, $N_D = 5\times10^{17}$ cm^{-3}; p-type absorber $x_{Cd} = 0.19$, $N_A = 10^{17}$ cm^{-3}; P$^+$ barrier $x_{Cd} = 0.25−0.45$, $N_A = 10^{17}$ cm^{-3}; n$^+$ contact $x_{Cd} = 0.19$, $N_D = 10^{17}$ cm^{-3}.

The energy band profile calculated for the p type active layer $N_A = 10^{17}$ cm^{-3} ($N_A > 3n_i \sim 3.6 \times 10^{16}$ cm^{-3}) and $T = 300$ K is presented in Fig. 2a. Composition and doping gradients at the interface between the N$^+$ contact and p-type doped active layers were chosen in order not

to generate discontinuities in the energy band profile among main constituent heterojunctions of the $N^+pP^+n^+$ structure. The electric field drops mostly on that interface ($E \sim 15 \times 10^3$ V/cm), which is shown in Fig. 2b. In addition, the electric field dependence on P^+ barrier composition ($x_{Cd} = 0.25-0.45$) is also shown pointing out that the P^+ layer x_{Cd} marginally contributes to the electric field drop along the structure. It is clearly visible that for zero bias condition the electric field does not drop on the active layer, meaning that the response time is fundamentally limited by diffusion of the photo-generated carriers.

Both absorber's doping N_A and absorber's thickness d have a significant impact on the response time. The absorber's doping influence on the response time is presented in Fig. 3a. The absorber thickness $d = 1$ µm and no extra series resistance ($R_{S+} = 0$ Ω) were assumed in simulations. The response time decreases from ~ 1.8 ns to ~ 1 ns for the absorber's doping $N_A = 5 \times 10^{15}-10^{17}$ cm^{-3}. To compare those results with the diffusion time we assume that an electron to hole mobility ratio ~ 100 (for $x_{Cd} = 0.19$, $N_A = 5 \times 10^{15}$ cm^{-3} an ambipolar diffusion coefficient and ambipolar diffusion length are $D_a = 5.6 \times 10^{-4}$ m^2/s and $L_a = 2.16$ µm, respectively, while for $N_A = 10^{17}$ cm^{-3} – they are $D_a = 2.73 \times 10^{-3}$ m^2/s, $L_a = 4.08$ µm, for $T = 300$ K). The diffusion time is given by $- \tau_{diff} = \frac{d^2}{2.4 D_a}$ for $d << L_a$ and changes from 0.74 ns to 0.15 ns for $N_A = 5 \times 10^{15}-10^{17}$ cm^{-3}. That confirms that highly doped p-type material significantly reduces the diffusion time. Another factor contributing to the response time is the RC constant τ_{RC}. The structure capacitance C and series resistance R_S, presented in Fig. 3b, were assessed at levels of ~ 0.18 nF and 0.77 Ω, resulting in extra $\tau_{RC} \sim 0.14$ ns for $N_A = 10^{17}$ cm^{-3} and $\tau_{RC} \sim 0.19$ ns for $N_A = 5 \times 10^{15}$ cm^{-3}, respectively. The diffusion time τ_{diff} and time constant τ_{RC} are shown in Fig. 3a and in the whole absorber's doping range they have smaller values than the response time.
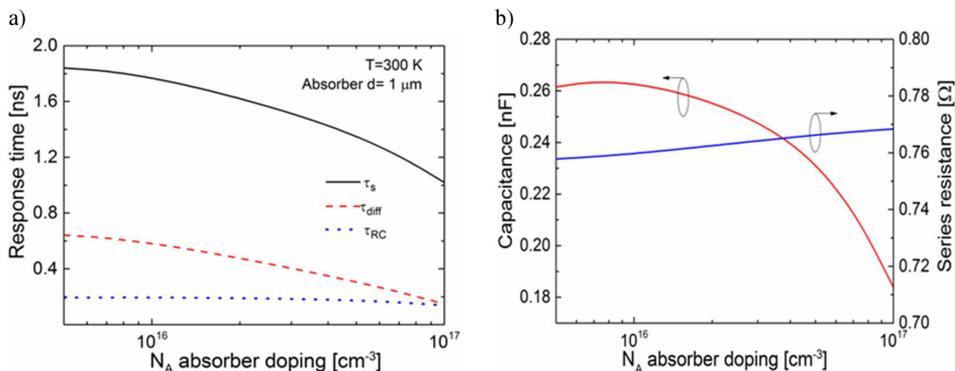

Fig. 3. Response time, diffusion time and RC constant calculated for $T = 300$ K versus absorber's doping $N_A = 5 \times 10^{15}-10^{17}$ cm^{-3} (a). Structure capacitance and resistance versus absorber's doping (b).

The diffusion time depends on the distance range between the generation and depletion areas, meaning that the response time will be suppressed with a reduction of active layer thickness. Assuming the absorber's thickness $d = 1-5$µm, active layer doping $N_A = 10^{17}$ cm^{-3} and no extra resistance contribution ($R_{S+} = 0$ Ω), the response time stays within a range $\tau_s \sim 1-3.08$ ns but the diffusion time reaches $\tau_{diff} = 0.15-2.35$ ns, as it is shown in Fig. 4a. The RC constant calculated for the data presented in Fig. 4 (b) reaches $\tau_{RC} \sim 0.14-0.24$ ns for $d = 1-5$ µm, respectively.
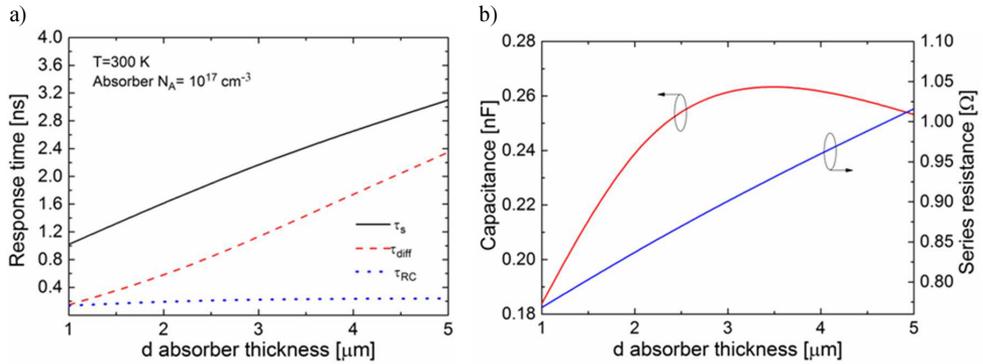
Fig. 4. Response time, diffusion time and RC constant calculated for $T = 300$ K versus absorber's thickness $d = 1-5$ μm for absorber's doping $N_A = 10^{17}$ cm^{-3} (a). Capacitance and resistance versus absorber d (b).

The dependencies of responsivity and detectivity on absorber's doping and absorber's thickness are presented in Fig. 5. The maximum detectivity was found at the level of $\sim 2.5 \times 10^9$ cmHz$^{1/2}$/W for the absorber doping $N_A = 10^{17}$ cm^{-3} (that nearly corresponds to $N_A \sim 3n_i$ being an optimal value where Auger thermal generation reaches its minimal value) for $d = 1$ μm and for $T = 300$ K, what is shown in Fig. 5a. The maximum detectivity increases with absorber's thickness and reaches its maximum value for absorber's thickness $d \sim 3.5$ μm, what is presented in Fig. 5b. The response time at a level of 1 ns can be obtained for the optimum absorber's thickness $d = 1$ μm and absorber's doping $N_A = 10^{17}$ cm^{-3} with detectivity greater than $\sim 2.5 \times 10^9$ cmHz$^{1/2}$/W.
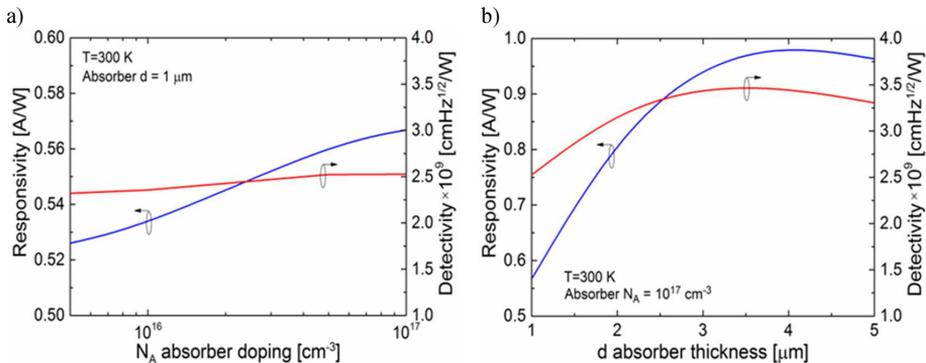

Fig. 5. Responsivity and detectivity versus absorber's doping for absorber's thickness $d = 1$ μm (a). Responsivity and detectivity versus absorber's thickness, absorber's doping $N_A = 10^{17}$ cm^{-3} (b).

In the whole simulation of the absorber's contribution, the response time was higher than the diffusion time and RC constant (see Figs. 3a and 4a). In order to clarify these differences an impact of other constituent layers of the heterojunction on the photodetector's response time was analysed. The dependence of the response time and detectivity on the N$^+$ contact layer thickness within a range $d = 2-20$ μm was calculated. The N$^+$ contact thickness marginally contributes to the response time. For $d > 9$ μm the response time saturates reaching 0.98 ns, what is shown in Fig. 6a. The shorter N$^+$ contact layer the slightly higher response is reached ($\tau_s \sim 1.34$ ns was assessed for $d = 2$ μm). Within a range $d = 1.5-9$ μm of the N$^+$ layer thickness, the response time could be increased by 350 ps, what is shown in Fig. 6a. D^* also stays constant

www.czasopisma.pan.pl   PAN   www.journals.pan.pl
POLSKA AKADEMIA NAUK
P. Martyniuk, M. Kopytko, et al.: THEORETICAL SIMULATION OF A ROOM TEMPERATURE ...

within the analysed N^+ contact layer thickness reaching $\sim 2.5 \times 10^9$ cmHz$^{1/2}$/W, what is presented in Fig. 6b.

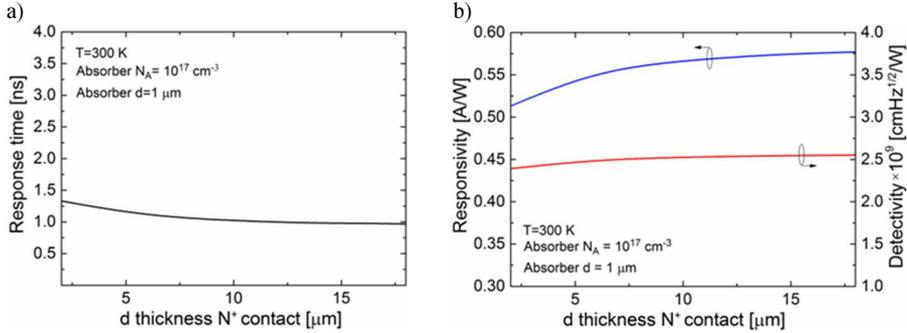Fig. 6. Response time calculated for $T = 300$ K versus N^+ thickness contact layer $d = 2-20$ μm, absorber's doping $N_A = 10^{17}$ cm^{-3} (a). Responsivity and detectivity versus N^+ thickness contact layer, absorber's thickness $d = 1$ μm, absorber's doping $N_A = 10^{17}$ cm^{-3} (b).

The N^+ contact layer must be transparent for IR and must be chosen properly in relation to the active layer regarding its composition and thickness (resistance − mesa structure). Doping must be high $N_D > 10^{17}$ cm^{-3} to make the metallization to that layer. The higher composition the slightly higher response time is reached, however x_{Cd} marginally contributes to τ_s, meaning that lowering x_{Cd} to a level slightly higher than the active layer enables to decrease τ_s by ~ 220 ps for the N^+ contact layer doping $N_D = 5 \times 10^{17}$ cm^{-3}, what is presented in Fig. 7a. The N^+ layer x_{Cd} has also a marginal influence on detectivity reaching $\sim 2.5 \times 10^9$ cmHz$^{1/2}$/W, what is shown in Fig. 7b.
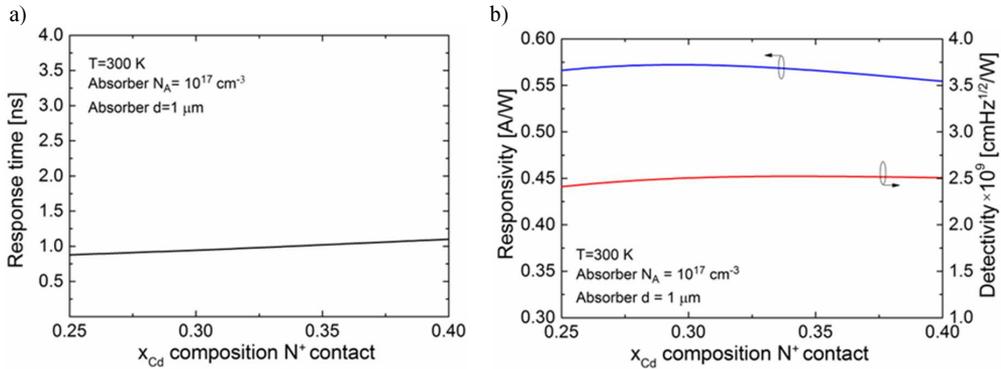

Fig. 7. Response time calculated for $T = 300$ K versus N^+ contact layer composition $x_{Cd} = 0.25-0.4$, absorber's doping $N_A = 10^{17}$ cm^{-3} (a). Responsivity and detectivity versus N^+ contact layer x_{Cd} composition, absorber's doping $N_A = 10^{17}$ cm^{-3} (b).

The contribution of the P^+ barrier composition within a range $x_{Cd} = 0.2-0.45$ to τ_s and D^* was simulated. The P^+ barrier composition should be at a level of $x_{Cd} < 0.35$ to reach an ultra-short response time $\tau_s < 1$ ns for an extra series resistance $R_{S+} = 0$ Ω, what is presented in Fig. 8a. P^+ x_{Cd} has a significant influence on detectivity, what is shown in Fig. 8b. For P^+ $x_{Cd} < 0.4$ the detectivity D^* decreases rapidly for analysed conditions, its maximum value being

www.czasopisma.pan.pl   PAN   www.journals.pan.pl
POLSKA AKADEMIA NAUK

Metrol. Meas. Syst., Vol. 24 (2017), No. 4, pp. 729–738.

$D^* \sim 3.3 \times 10^9$ cmHz$^{1/2}$/W for $x_{Cd} = 0.45$, whereas for the x_{Cd} comparable to the active layer D^* reaches $\sim 1.25 \times 10^9$ cmHz$^{1/2}$/W assuming $R_{S+} = 0$ Ω.

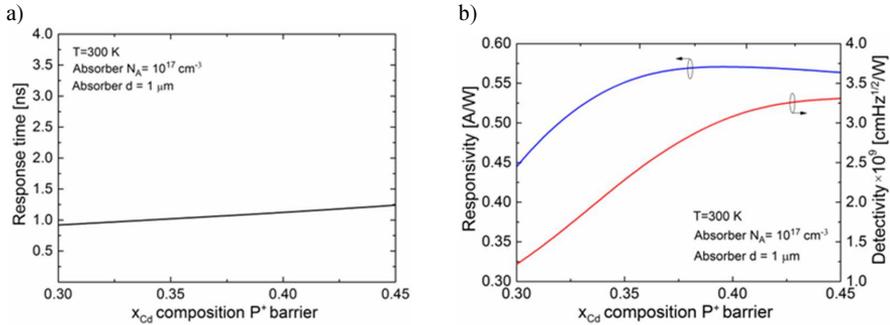Fig. 8. Response time calculated for $T = 300$ K versus P$^+$ barrier layer composition $x_{Cd} = 0.3–0.45$, absorber's doping $N_A = 10^{17}$ cm^{-3} (a). Responsivity and detectivity versus P$^+$ barrier layer x_{Cd} composition, absorber's doping $N_A = 10^{17}$ cm^{-3} (b).

The influence of the P$^+$ barrier layer doping within a range $N_A \sim 5 \times 10^{15}–5 \times 10^{17}$ cm^{-3} on τ_s and D^* is presented in Figs. 9a and 9b. The shortest response time $\tau_s \sim 0.7$ ns was reached for $N_A \sim 5 \times 10^{17}$ cm^{-3} doping being higher than doping of the absorber layer ($N_A = 10^{17}$ cm^{-3}). The P$^+$ barrier doping highly influences both responsivity and detectivity characteristics. Once the P$^+$ barrier doping increases within a range $N_D = 5 \times 10^{15} – 5 \times 10^{17}$ cm^{-3}, the detectivity changes from $\sim 7.6 \times 10^8$ to $\sim 3.3 \times 10^9$ cmHz$^{1/2}$/W. The optimal value of P$^+$ barrier layer doping should be greater than $N_A = 10^{17}$ cm^{-3}.
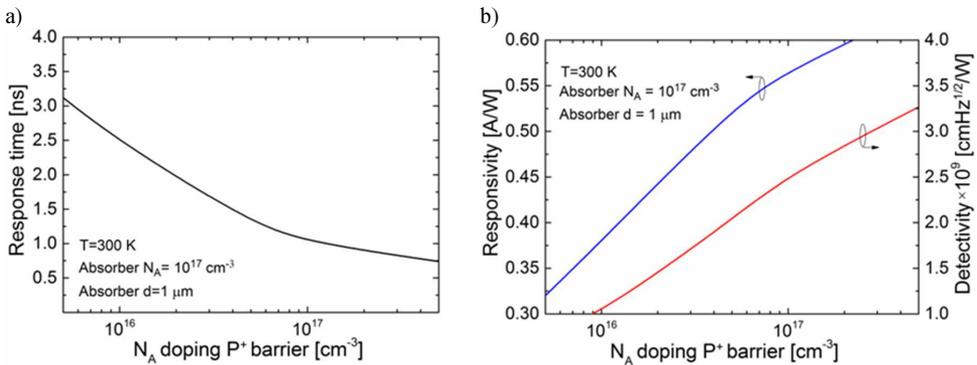

Fig. 9. Response time calculated for $T = 300$ K versus P$^+$ barrier layer doping $N_A = 5 \times 10^{15} – 5 \times 10^{17}$ cm^{-3}, absorber's doping $N_A = 10^{17}$ cm^{-3} (a). Responsivity and detectivity versus P$^+$ barrier layer doping, absorber's doping $N_A = 10^{17}$ cm^{-3} (b).

The influence of the P$^+$ barrier layer thickness within a range $d = 0.5–3$ μm on τ_s and D^* was simulated. Increasing the P$^+$ barrier width causes a very small increase in the response time and has also a small effect on both response time and detectivity, what is shown in Figs. 10a and 10b. The response time changes from to ~ 1 to ~ 1.1 ns for $d = 0.5–3$ μm. The response time $\tau_s \leq 1$ ns could be reached for the P$^+$ barrier thickness $d < 1$ μm, for the absorber's doping $N_A = 10^{17}$ cm^{-3} assuming no extra R_{S+}. D^* stays constant within the analysed P$^+$ barrier layer range reaching $\sim 2.5 \times 10^9$ cmHz$^{1/2}$/W.
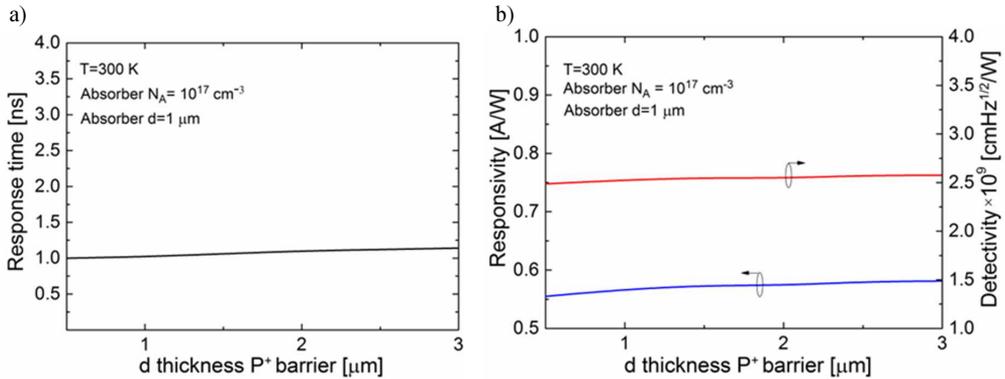
a)

b)

Fig. 10. Response time calculated for $T = 300$ K versus P$^+$ barrier thickness $d = 0.5-3$ μm, absorber's doping $N_A = 10^{17}$ cm^{-3} (a). Responsivity and detectivity versus P$^+$ barrier thickness d, absorber's doping $N_A = 10^{17}$ cm^{-3} (b).

The influence of the thickness of *n*-type interface layer $d = 0.4-2$ μm between N$^+$ contact and absorber on both τ_s and D^* is presented in Figs. 11a and 11b. The *n*-type interface thickness d has almost any contribution to the response time. For $0.4 < d < 2$ μm the response time increases only by ~ 130 ps, whereas D^* reaches $\sim 2.5 \times 10^9$ cmHz$^{1/2}$/W in the analysed *n*-type interface thickness range.
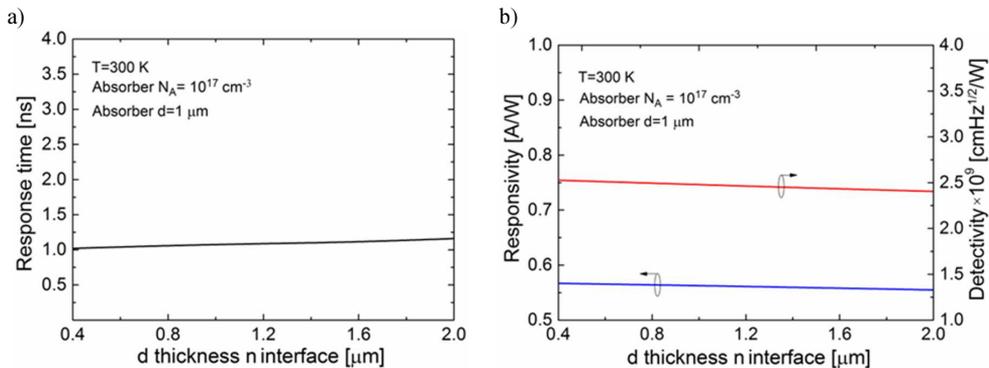
a)

b)

Fig. 11. Response time calculated for $T = 300$ K versus *n* type interface thickness $d = 0.4-2$ μm, absorber's doping $N_A = 10^{17}$ cm^{-3} (a). Responsivity and detectivity versus *n* type interface thickness d, absorber's doping $N_A = 10^{17}$ cm^{-3} (b).

The extra series resistance related to the processing, R_{S+}, plays a decisive role in increasing the response time. The absorber thickness $d = 1$ μm and extra series resistance from within a range $R_{S+} = 0-10$ Ω were assumed in simulations. The influence of the absorber's doping on the response time is presented in Fig. 12. The extra $R_{S+} = 10$ Ω increases the response time more than two times, i.e. for the absorber's $N_A = 10^{17}$ cm^{-3} the response time changes within a range $\tau_s \sim 2.3-1$ ns.

www.czasopisma.pan.pl   PAN   www.journals.pan.pl
POLSKA AKADEMIA NAUK

Metrol. Meas. Syst., Vol. 24 (2017), No. 4, pp. 729–738.
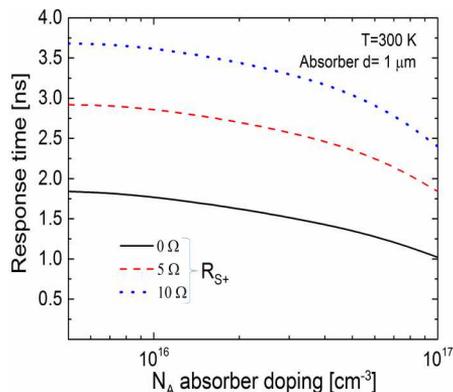
Fig. 12. Response time calculated for $T = 300$ K versus absorber's doping $N_A = 5 \times 10^{15} - 10^{17}$ cm^{-3}, extra $R_{S+} = 0 - 10$ Ω. Absorber's thickness $d = 1$ μm.

3. Conclusion

A structure operating in room temperature enabling to reach the response time $\tau_s < 1$ ns and detectivity $D^* > 2 \times 10^9$ cmHz$^{1/2}$/W was presented. The greatest impact on the response time is that of physical parameters of the active layer and P$^+$ barrier layer. Other layers have a marginal influence on both response time and detectivity. An optimal LWIR absorber $x_{Cd} = 0.19$ should meet following requirements: $N_A > 10^{17}$ and $d \leq 1$ μm. N$^+$ contact layer thickness $d \geq 10$ μm and $x_{Cd} < 0.35$. P$^+$ barrier layer $x_{Cd} \leq 0.35$, doping $N_A \geq 10^{17}$cm^{-3} and thickness d ≤ 2 μm. Assuming an extra series resistance $R_{S+} = 10$ Ω the response time increases to 2.3 ns.

Acknowledgments

References

[1] Rogalski, A. (2011). *Infrared Detectors*. 2nd ed. CRC Press, Boca Raton.

[2] Wojtas, J., Bielecki, Z., Stacewicz, T., Mikołajczyk, J., Nowakowski, M. (2012). Ultrasensitive laser spectroscopy for breath analysis. *Opto-Electron. Rev.*, 20, 26–39.

[3] Elliot, C.T., Gordon, N.T., Hall, R.S., Phillips, T.J., Jones, C.L., Best, A. (1997). 1/f noise studies in uncooled narrow gap Hg$_{1-x}$Cd$_x$Te non-equilibrium diodes. *J. Electron. Mater.*, 25, 643–648.

[4] Kopytko, M., Jóźwikowski, K., Madejczyk, P., Pusz, W., Rogalski, A. (2013). Analysis of the response time in high-temperature LWIR HgCdTe photodiodes operating in non-equilibrium mode. *Infrared Phys. Technol.*, 61, 162–166.

[5] Kopytko, M., Jóźwikowski, K., Rogalski, A., Jóźwikowska, A. (2010). High frequency response of near-room temperature LWIR HgCdTe heterostructure photodiodes. *Opto-Electron. Rev.*, 18, 277–283.

[6] Pawluczyk, J., Piotrowski, J., Pusz, W., Koźniewski, A., Orman, Z., Gawron, W., Piotrowski, A. (2015). Complex behavior of time response of HgCdTe HOT photodetectors. *J. Electron. Mater.*, 44, 3163–3173.

[7] Madejczyk, P., Gawron, W., Martyniuk, P., Kębłowski, A., Piotrowski, A., Pusz, W., Kowalewski, A., Piotrowski, J., Rogalski, A. (2013). MOCVD grown HgCdTe device structure for ambient temperature LWIR detectors. *Semicond. Sci. Technol.*, 28, 105017, 1–7.

[8] Madejczyk, P., Gawron, W., Martyniuk, P., Kębłowski, A., Pusz, W., Pawluczyk, J., Kopytko, M., Rutkowski, J., Rogalski, A., Piotrowski, J. (2017). Engineering steps for optimizing high temperature LWIR HgCdTe photodiodes. *Infrared Phys. Technol*., 81, 276–281.

[9] Rogalski, A. (2005). HgCdTe infrared detector material: history, status and outlook. *Rep. Prog. Phys.*, 68, 2267–2336.

[10] Ashley, T., Elliott, C.T. (1985). Non-equilibrium mode of operation for infrared detection. *Electron. Lett.*, 21, 451–452.

[11] Elliot, C.T., Gordon, N.T., Hall, R.S., Philips, T.J., White, A.M., Jones, C.L., Maxey, C.D., Metcalfe, N.E. (1996). Recent results on MOVPE grown heterostructure devices. *J. Electron. Mater.*, 25, 1139–1145.

[12] Emelie, P.Y., Philips, J.D., Velicu, S., Grein, C.H. (2007). Modeling and design consideration of HgCdTe infrared photodiodes under non equilibrium operation. *J. Electron. Mater.*, 36, 846–851.

[13] Emelie, P.Y., Velicu, S., Grein, C.H., Philips, J.D., Wijewarnasuriya, P.S., Dhar, N.K. (2008). Modeling of LWIR HgCdTe Auger-suppressed infrared photodiodes under non equilibrium operation. *J. Electron. Mater.*, 37, 1362–1368.

[14] Piotrowski, A., Piotrowski, J., Gawron, W., Pawluczyk, J., Pędźinska, M. (2009). Extension of spectral range of Peltier cooled photodetectors to 16 μm. *Proc. SPIE*, 7298, 729824.

[15] Stanaszek, D., Piotrowski, J., Piotrowski, A., Gawron, W., Orman, Z., Paliwoda, R., Brudnowski, M., Pawluczyk, J., Pędzińska, M. (2009). Mid and long infrared detection modules for picosecond range measurements. *Proc. SPIE*, 7482, 74820M-74820M-11.

[16] Piotrowski, J., Pawluczyk, J., Piotrowski, A., Gawron, W., Romanis, M., Kłos, K. (2010). Uncooled MWIR and LWIR photodetectors in Poland. *Opto-Electron. Rev.*, 18, 318–327.

[17] Velicu, S., Grein, C.H., Emelie, P.Y., Itsuno, A., Philips, J.D., Wijewarnasuriya, P. (2010). MWIR and LWIR HgCdTe infrared detectors operated with reduced cooling requirements. *J. Electron. Mater.*, 39, 873–881.

[18] APSYS Macro/User's Manual ver. 2011. (2011). Crosslight Software, Inc.

[19] Capper, P.P. *Properties of narrow gap cadmium-based compounds.* London, U.K.: Inst. Elect. Eng.

[20] Wenus, J., Rutkowski, J., Rogalski, A. (2001). Two-dimensional analysis of double-layer heterojunction HgCdTe Photodiodes. *IEEE Trans. Electron Devices*, 48, 7, 1326−1332.

[21] Li, Q., Dutton, R.W. (1991). Numerical small-signal AC modeling of deep-level-trap related frequency-dependent output conductance and capacitance for GaAs MESFET's on semi-insulating substrates. *IEEE Trans. Electron Devices*, 38, 1285–1288.